ACS OMEGA

http://pubs.acs.org/journal/acsodf

Article

Facile Microwave Synthesis of Hierarchical Porous Copper Oxide and Its Catalytic Activity and Kinetics for Carbon Monoxide Oxidation

Abdallah F. Zedan,* Amina S. AlJaber, and M. Samy El-Shall*

Cite This: *ACS Omega* 2022, 7, 44021−44032

Read Online

ACCESS | Metrics & More | Article Recommendations | Supporting Information

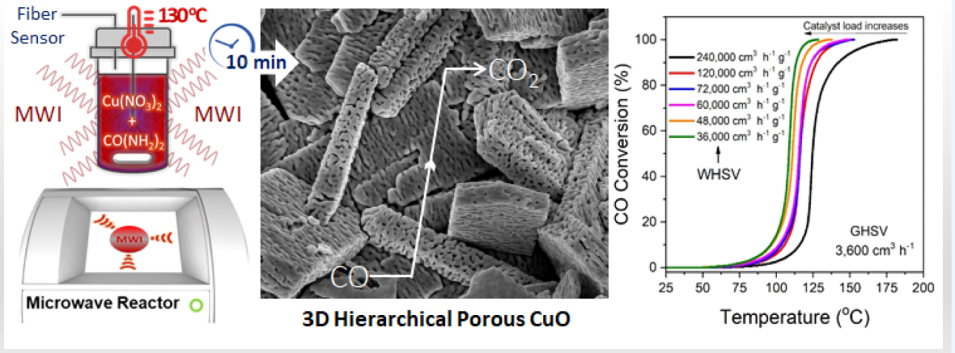

ABSTRACT: The synthesis of copper oxide (CuO)-based nanomaterials has received a tremendous deal of interest in recent years. Particularly, the design and development of novel CuO structures with improved physical and chemical properties have attracted immense attention, especially for catalysis applications. We report on a rational, rapid, and surfactant-free microwave synthesis (MWS) of hierarchical porous copper oxide (HP-CuO) with a three-dimensional (3D) sponge-like topology using an MWS reactor. The activity of the microwave (MW)-synthesized HP-CuO catalysts for carbon monoxide (CO) oxidation was studied and compared to CuO prepared by the conventional heating method (CHM). Results showed that HP-CuO catalysts prepared by MWS for 10 and 30 min surpassed the CuO catalyst prepared by CHM, exhibiting T_{80} of 98 and 115 °C, respectively, as compared to 185 °C of CuO prepared by CHM (T_{80} is the temperature corresponding to 80% CO conversion). In addition, the MW-synthesized HP-CuO catalysts outperformed the CHM-synthesized CuO, achieving a 100% CO conversion at 150 °C compared to 240 °C in the case of CuO prepared by CHM. Interestingly, the HP-CuO catalyst expressed workable CO conversion kinetics with a reaction rate of c.a.35 μmol s^{-1} g^{-1} at 150 °C and apparent activation energy (E_a) of 82 kJ mol^{-1}. The HP-CuO catalyst showed excellent cycling and long-term stabilities for CO oxidation up to 4 cycles and 72 h on the stream, respectively. The enhanced catalytic activity and stability of the HP-CuO catalyst appear to result from the unique topological and structural features of HP-CuO, which were revealed by SEM, XRD, Raman, BET, TGA, XPS, and TPR techniques.

1. INTRODUCTION

Over the past years, numerous studies have been conducted on heterogeneous catalysts and their applications for environmental remediation. The catalyzed oxidation of carbon monoxide (CO) is a crucial procedure for the removal of toxic CO in fuel emissions and automobile industries. It is also critical for some industrial applications such as the removal of poisoning CO in fuel cells and carbon dioxide lasers.[1] Supported precious metals including Au, Pt, Pd, Ir, and Ru are key components of many active catalysts for CO oxidation.[2,3] Nevertheless, exploring efficient and cost-effective catalysts remains a crucial demand for environmental sustainability. This demand could be reached by developing non-precious materials with improved physical and chemical properties for enhanced catalytic activity.[4] Copper (Cu) is an earth-abundant, inexpensive, and major industrial transition metal. In recent years, Cu-based materials have been extensively studied for basic and applied research in various sectors. Nanoarchitectures of copper oxide (CuO) is the trending form of Cu that have attracted immense attention for several applications such as gas separation, chemical- and biochemical sensing, solar cells, energy conversion, and catalysis.[5] They constitute an important class of transition

Received: August 22, 2022
Accepted: November 9, 2022
Published: November 17, 2022

metal nanomaterials of low cost and environmental impact with widespread potential applications, especially in environmental heterogeneous catalysis.[6−9] The morphology and microstructure of heterogeneous catalysts are among the main determinants of their physicochemical properties and hence their catalytic activity.[10] As such, the rational design and synthesis of CuO structures with controlled architectures and properties have received great efforts toward enhanced catalytic performance.[11−14]

CuO can be synthesized using various physical and chemical methods such as laser ablation, ball milling, arc discharge, chemical reduction, microemulsion, sonochemical, photochemical, electrolysis, thermal decomposition, combustion, hydrothermal, and microwave synthesis methods.[15] Among these, microwave synthesis (MWS) is a rapid, efficient, and cost-effective technique for the fabrication of a wide range of inorganic nanostructures with tailored structures and compositions. It has received tremendous attention in the field of synthetic chemistry due to its fairly simple, low-cost, and large-scale production merits. MWS allows the fast nucleation and growth of nanoscale materials from their precursors in various aqueous and non-aqueous environments.[16,17] The MWS intercedes via energy transfer as microwave irradiation (MWI) to the reactants through mechanisms of ionic conduction and dipole moment rotation. This results in an instantaneous temperature rise and decreased activation energy, leading to rapid decomposition of the precursor molecules.[18,19]

CuO catalysts have shown promise for catalytic CO oxidation reactions, and controlling the surface and morphological properties can potentially lead to the improvement of their catalytic activity.[20−22] The MWS should be considered an effective and economic synthetic approach to achieve these goals.[23,24] In this report, we present a simple, rapid, facile, and surfactant-free microwave (MW)-driven method for the rational synthesis of hierarchical porous CuO (HP-CuO) with a three-dimensional (3D) sponge-like morphology and investigate their catalytic performance for CO oxidation. To the best of the authors' knowledge, this is the first report to prepare hierarchical porous copper oxide bearing a sponge-like morphology from an aqueous mixture of copper nitrate and carbamide precursors by MWI in a closed vial at 130 °C using an MWS reactor. The MW-synthesized HP-CuO catalysts were characterized using FE-SEM, XRD, Raman, BET, TGA, H_2-TPR, and CO-TPR techniques. The catalytic activity, kinetics, and stability of the MW-synthesized HP-CuO catalysts for CO oxidation have been investigated and compared to CuO catalysts prepared using the conventional heating method (CHM). The obtained results suggest that the described MWS unfolds a simple approach to obtain HP-CuO, which paves the way for efficient, stable, and low-cost catalysts for low-temperature catalytic CO oxidation.

2. MATERIALS AND METHODS

2.1. Materials. Chemical reagents were purchased and used as received, including copper(II) nitrate trihydrate ($Cu(NO_3)_2{\cdot}3H_2O$, purum grade, 98%, Sigma-Aldrich) and urea (also known as carbamide, $CO(NH_2)_2$, purum grade, >99.0%, Fluka). The water used in all experiments was ultrapure deionized water by Direct-Q 5UV (Millipore).

2.2. Methods. *2.2.1. Microwave Synthesis of Hierarchical Porous Copper Oxide.* Hierarchical porous copper oxide (HP-CuO) was synthesized by MWS in a closed vial under mild temperature and pressure using an MWS reactor. In a typical MWS of HP-CuO, equal volume portions of aqueous solutions of carbamide ($CO(NH_2)_2$, 4 mol L^{-1}, 0.04 mol) and copper nitrate ($Cu(NO_3)_2{\cdot}3H_2O$, 0.5 mol L^{-1}, 0.005 mol) were mixed in a sealable and microwaveable reaction vial (G30, Glass, 30 mL max., Anton-Paar). The reaction vial was equipped with a small magnet bar for mechanical stirring during the microwave irradiation (MWI) and was then closed with a standard-fit cap and sealing septum. The reaction vial was transferred into the cavity of an MWS reactor (Monowave 300, Anton-Paar GmbH) that was equipped with an in situ temperature probe to monitor the sample's temperature. The vial with the reaction mixture inside the MWS reactor cavity was heated to 130 °C by MWI for a predetermined exposure time (1−30 min) under continuous magnetic stirring (1200 rpm). Upon reaction completion, the mixture was cooled down to 55 °C under stirring and was then removed from the MWS reactor cavity. The product was separated by a centrifuge at 5000 rpm for 15 min and was repeatedly washed with DI water for three washing/centrifuge cycles. The product was dried in an oven (Isotemp-282A, Fisher Sci., US) at 80 °C for 12 h. The effect of the microwave irradiation (MWI) time on the surface topology of HP-CuO was investigated by changing the MWI time to 1, 2, 4, 10, and 30 min. For comparison, CuO was also prepared from the same reaction mixture of copper nitrate and carbamide using a conventional heating method (CHM) under similar hydrothermal conditions. For all MWS and CHM experiments, the molar ratio of carbamide and copper nitrate starting materials was maintained at a fixed ratio of 8. The yield of CuO prepared by the MWS using a reaction mixture with a total volume of 20 mL was >90% based on the metal precursor. All samples prepared by MWS and CHM were annealed at 400 °C for 2 h at a heating ramp rate of 5 °C min^{-1} in static air using a muffle furnace (Nabertherm B170, Germany).

2.2.2. Characterization. The prepared materials were characterized by using field-emission scanning electron microscopy (FE-SEM), X-ray diffraction (XRD), Raman, physisorption (BET), thermal gravimetric analysis (TGA), X-ray photoelectron spectroscopy (XPS), and temperature-programmed reduction (TPR) techniques. FE-SEM micrograph images were collected by using NOVA 450 (NANO-SEM, FEI, Czech Republic). XRD patterns were recorded at 30 kV and 20 mA by using a MiniFlex II powder diffractometer (Rigaku, Japan) equipped with Cu $K_{\alpha 1}$ radiation. The crystal structures of the prepared samples were indexed based on the JCPDS-ICCDD database system. Raman spectroscopy measurements were performed using a DXR-2 Raman microscope (Thermo Fisher Sci., USA) that is equipped with a laser source of 780 nm wavelength for excitation. The settings for the collection of the spectra involved 20 accumulations, a total acquisition time of 5 min, a spectral grating resolution of 4 cm^{-1}, and a laser power of 5 mW. Physisorption measurements of nitrogen (N_2) adsorption−desorption isotherms were performed at 77 K in the relative pressure (P/P_O) range of 0.05−1 using an ASAP 2460 surface area analyzer (Micromeritics, USA). Before physisorption measurements, samples were degassed by two-stage heating, first at 90 °C for 1 h and then at 150 °C for another 1 h in an N_2-He atmosphere. The specific surface area (SSA) was calculated by using the BET method. TGA measurements were carried out using Pyris 6 analyzer (PerkinElmer, Netherlands), and the sample was heated in static air up to 700 °C with a heating ramp rate of 10 °C min^{-1}. H_2-TPR measurements were performed using

https://doi.org/10.1021/acsomega.2c05399
ACS Omega 2022, 7, 44021−44032

Chemisorb 2750 equipped with ChemiSoft TPx and TCD (Micromeritics, USA). For a typical H_2-TPR measurement, 50 mg of the sample was heated up to 400 °C at a heating rate of 10 °C min^{-1} and under a constant flow of 30 mL min^{-1} of 10% H_2/Ar gas mixture. CO-TPR measurements were carried out using a customized experimental setup adopting an infrared gas detector to probe the CO consumption. For a typical CO-TPR measurement, 50 mg of the sample was heated up to 200 °C at a heating rate of 5 °C min^{-1} under a constant flow of 50 mL $min^{-1}$of 10% CO/He gas mixture. XPS spectra were recorded under ultra-high-vacuum (UHV) conditions using AXIS Ultra spectrometer (KRATOS Analytical, UK).

2.2.3. Catalytic Activity, Kinetics, and Stability Measurements. The catalytic activity of the prepared samples was studied for carbon monoxide (CO) oxidation. Catalytic CO oxidation measurements were carried out using a custom-built catalytic reactor described in detail earlier.[3] The reactor comprised a horizontal quartz tube, a split tube furnace, and an infrared flue gas detector. In a typical experiment, 50 mg of the catalyst was charged into a fixed bed inside the reactor tube. The catalyst temperature was monitored by a thermocouple inserted inside the reactor tube in direct contact with the sample, and temperature was logged using a multifunction DAQmx interface (USB-6008, National Instruments, USA). A feed-in gas mixture comprising 4 vol % CO, 20 vol % O_2, and an Ar balance was passed over the sample continuously at a constant flow rate of 60 cm^3 min^{-1}. The weight hourly space velocity (WHSV) was maintained at 72,000 cm^3 g^{-1} h^{-1} by using a set of digital mass flow controllers (HI-TEC, Bronkhorst). The temperature of the catalyst was increased at a constant heating ramp rate of 5 °C/min. The feed-out gas was passed into a multichannel infrared (IR) gas analyzer for CO detection (model IR200, Yokogawa, Japan). The data were logged with LabVIEW software, and the catalytic activity of the catalysts was expressed as % CO conversion. The kinetic measurements of CO oxidation over a selected catalyst were carried out as reported earlier.[25] Typically, the CO conversion was studied at various temperatures and catalyst loadings while maintaining constant molar flow rates corresponding to a gas hourly space velocity (GHSV) of 3600 cm^3 h^{-1}. The CO oxidation rates and apparent activation energy were calculated as described earlier. The cycling stability and long-term stability at 150 ± 5 °C of a selected catalyst were carried out for up to 4 cycles and 72 h under a continuous stream, respectively.

3. RESULTS AND DISCUSSION

MWS is a powerful synthetic approach that has gained tremendous attention in the field of synthetic chemistry. It is widely accepted as a widespread, energy-efficient, eco-friendly, and fast synthetic method.[23,26] Unlike conventional heating methods, microwave irradiation (MWI) simply satisfies the goal of being an abrupt, fast, and homogenous heat-driving method. MWI can cause instantaneous and uniform heating of reaction mixtures, resulting in fast nucleation and growth of particles.[27] The MWS-based methods have been adopted for the fabrication of various nanoscale materials with a wide range of sizes, shapes, and phase characteristics.[27,28] The chemistry of MWS can typically result in higher rates of nanoparticle formation at shorter reaction times compared to CHMs. This gives the MWS the high merits of rapid and large-scale preparation. In this work, MWS was employed for the rapid and facile fabrication of hierarchical porous copper oxide (HP-CuO) using an MWS reactor (Monowave 300). The physical and chemical properties of the prepared materials were studied using standard imaging, spectroscopic, and characterization techniques.

Figure 1 displays the FE-SEM micrograph images of HP-CuO prepared by MWI in a closed vessel at 130 °C for 10 min

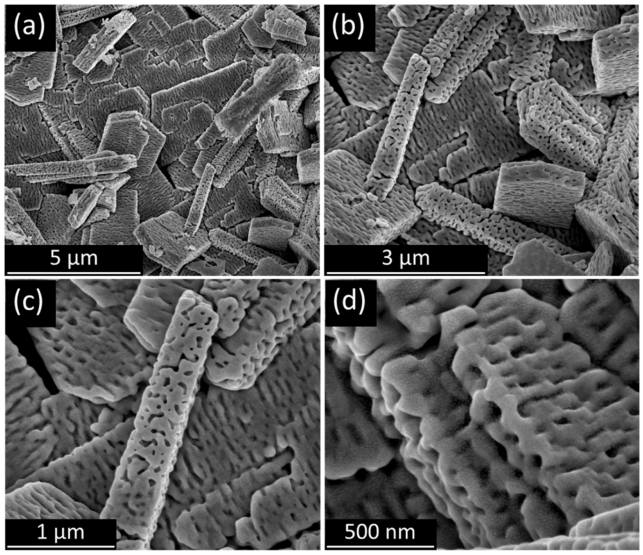

Figure 1. (a−d) FE-SEM images of hierarchical porous copper oxide (HP-CuO) prepared by MWS in a closed vessel at 130 °C under MWI for 10 min using a Monowave 300 MWS reactor.

using copper nitrate ($Cu(NO_3)_2$) and carbamide ($CO(NH_2)_2$) as the starting materials. The low- and high-magnification SEM images of HP-CuO shown in Figure 1 confirm the hierarchical porous texture and morphology of the MW-synthesized CuO nanostructures. The SEM images reveal a three-dimensional (3D) sponge-like surface topological structure of the MW-synthesized HP-CuO. The high-magnification SEM images (Figure 1c,d) show stacks of superlattice structures with ∼3−5 μm lateral dimensions, where each delicate 3D sponge-like stack is constructed of numerous sub-micrometer units assembled into platelet-like architectures with thicknesses ranging from ∼0.5−1 μm and an average lateral length of ∼3 μm. The SEM images of HP-CuO also show the HP-CuO porosity with open and interlaced pores which are joined together, forming plenty of cavities on the HP-CuO surface. It can be speculated that HP-CuO could express enhanced specific surface area (SSA) and a larger density of accessible active sites. This in turn can increase the contact area for specific gas adsorption and diffusion, and hence, the improvement of the catalytic performance of HP-CuO in gas-phase catalysis applications may ensue.[29] To confirm the role of MW-driven heating in the formation of HP-CuO, the synthesis was performed by CHM using a mixture of the same starting materials of copper nitrate and carbamide with the same 1:8 molar ratio. Figure S1 displays the FE-SEM images of the CuO particles prepared by CHM which reveal the formation of large CuO particles of irregular size and shape. The lack of hierarchy in the case of CuO prepared by CHM evidences the significance of MWI in forming HP-CuO.

To study the effect of the MWS conditions on the particle morphology, MWI time was varied as 1, 2, 4, 10, and 30 min using different reaction mixtures of the same composition and volume ratios. Figure 2 compares the FE-SEM images of the

https://doi.org/10.1021/acsomega.2c05399
ACS Omega 2022, 7, 44021−44032

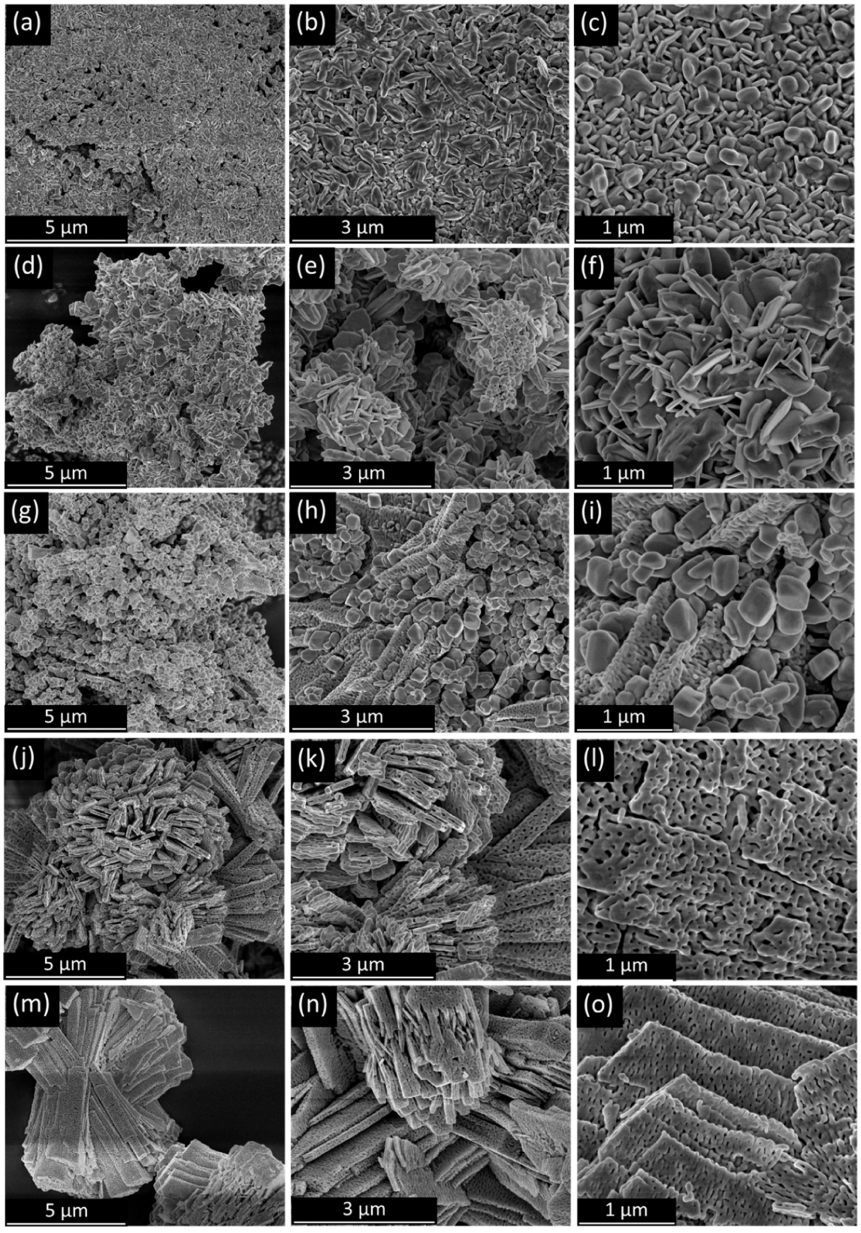

Figure 2. FE-SEM images of HP-CuO prepared by MWS in closed vials at 130 °C under different MWI times of (a−c) 1, (d−f) 2, (g−i) 4, (j−l) 10, and (m−o) 30 min, showing the effect of MWI time on CuO topology.

CuO samples prepared by MWS in closed vials at 130 °C under different MWI times of 1−30 min using an MWS reactor. The overall SEM images reveal the temporal evolution of the hierarchical porous (HP) structure of CuO while increasing the MWI time as 1, 2, and 4 min, as shown in Figure 2a−i. The SEM images of the CuO sample prepared by MWI for 1 and 2 min show particles with slightly irregular shapes and without visible porous features, as can be seen in Figure 2a−f, respectively. The CuO prepared by MWI for 4 min began expressing sub-micrometer features with primary pores (Figure 2g−i). When the MWI time was increased to 10 min, a complete growth of well-developed HP-CuO was reached, as shown in Figure 2j−l. Further increase of the MWI time to 30 min did not result in significant topological changes of HP-CuO, and comparable morphology to the HP-CuO synthesized with MWI for 10 min is observed. Only slightly larger assemblies of HP-CuO are manifested with stacked layers after MWI for 30 min.

The SEM results reveal the effect of MWI on the microstructure of HP-CuO with the formation of a superlattice structure for MWI times of 10−30 min. It is worth mentioning that our MWS is surfactant= free and that HP-CuO is obtained without using shape-directing or template agents, unlike those reported in the literature using pluronic acid, for example.[29] When $Cu(NO_3)_2$ is dissolved in water, the H_2O molecules could coordinate to Cu^{2+} cations using electrons in their bonding orbitals. This can weaken the hydroxyl group (O−H) bonds of water molecules bound onto the surface and lead to hydrolysis according to the pH of the mixture. The molar ratio of the copper nitrate and carbamide starting materials was adjusted to 1:8 so that carbamide will exist in the solution in excess and to assure oxide precipitation conditions. The instantaneous heating of the reaction mixture by MWI leads to

https://doi.org/10.1021/acsomega.2c05399
ACS Omega 2022, 7, 44021−44032

the hydrolysis of the carbamide molecules and the formation of ammonium cations (NH_4^+). This can increase the pH of the solution, which results in the precipitation of condensates of hydrated amorphous oxide.[30] The functionalities of MWI and carbamide for the construction of porous structures have been reported earlier by some other groups.[9,18,31,32] Since the CuO synthesized with carbamide using CHM did not express a hierarchical porous structure, it can be stated that MWS chemistry not only provided heat for carbamide hydrolysis by MWI but also offered chemical speciation orienting the growth of HP-CuO into 3D sponge-like architectures.[31]

The MWI could derive the alkalinization reaction of aqueous Cu(II) nitrate and carbamide and provide favorable thermodynamic and kinetic factors for the growth of HP-CuO under mild temperature and pressure. It triggered the formation of a porous network within the first few minutes of the reaction, and perfect HP-CuO could be obtained after MWI for 10 min. The difference between the porosity of CuO products obtained by the CHM and MWS appears to be related to the different hydrolysis and condensation rates of the reaction. The MWI enables the instantaneous heating of the reacting species and accelerates their supersaturation, nucleation, and reaction rates. Compared with CHM, MWS could provide faster hydrolysis and condensation events in a relatively very short time.[24,33,34] This could trigger the spontaneous formation of ultrafine CuO subunits followed by their instantaneous packing via self-assembly or oriented attachment to construct the HP-CuO with a 3D architecture and enhanced porosity.[34,35]

Powder X-ray diffraction (PXRD) is a powerful analytical tool for studying the crystal structure of solid materials.[36] Figure 3 presents the PXRD patterns of the MW-synthesized

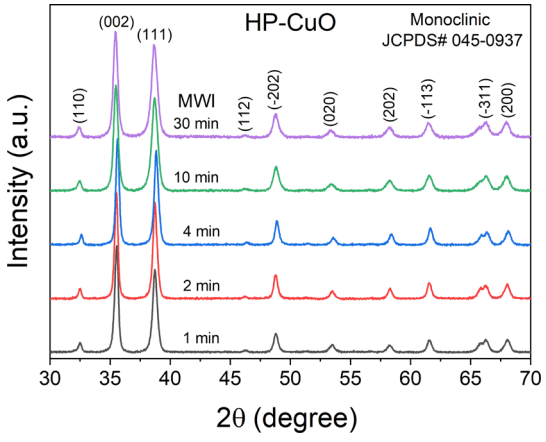

Figure 3. XRD patterns of different HP-CuO samples prepared by MWI for different times of 1−30 min in a closed vial at 130 °C using a microwave synthesis reactor.

HP-CuO samples prepared in closed vials at 130 °C by MWI for different times of 1−30 min. The XRD patterns of all MW-synthesized HP-CuO samples featured diffraction peaks typical of the monoclinic-structured copper oxide (JCPDS card no. 045-0937). These XRD peaks can be indexed to the (110), (002), (111), (112), (−202), (020), (202), (−113), (0311), and (200) planes characteristic of the polycrystalline CuO in the monoclinic $C2/c$ space group.[7] Similarly, the XRD pattern of the CuO prepared by the CHM that is displayed in Figure S2 shows a monoclinic structure similar to HP-CuO prepared by MWS.

Raman spectroscopy is a rapid, sensitive, and nondestructive technique to study the electronic properties and structure of ionic solids. As indicated by the XRD results, the MW-synthesized HP-CuO possessed a monoclinic structure with symmetry belonging to the $C2/c$ space group. Thus, each unit cell has 4 (Cu−O) molecules, and the primitive cell comprises 2 (Cu−O) units. Therefore, CuO exhibits 3 acoustic modes and 9 optical modes, with 3 optical modes being Raman active and 6 modes being infrared active. The 3 Raman-active modes ($2B_g$ and A_g) are correlated to the stretching and bending vibration of Cu−O.[25,37] The Raman spectrum of the MW-synthesized HP-CuO prepared under MWI for 10 min is shown in Figure S3. The Raman peak positioned at 300 cm^{-1} is ascribed to the A_g Raman mode which is characteristic of crystalline tenorite phase CuO.[37]

Figure 4 displays the multi-point nitrogen (N_2) adsorption−desorption isothermal plots (Figure 4a) and the thermal gravimetric (TGA) plots (Figure 4b) of CuO prepared by CHM and HP-CuO prepared by MWS under MWI for 10 min using MWS reactor. The N_2-isothermal plots of HP-CuO prepared by MWS and CuO prepared by CHM (Figure 4a) reveal type IV isotherms with hysteresis loops in the relative pressure range of 0.1−1.[13,38] The SSA values calculated using the BET method over the range $0.1 < P/P_o < 0.3$ for CuO and HP-CuO were determined as 4.3 and 10.4 m^2/g, respectively. The MW-synthesized HP-CuO exhibited an enhanced BET-SSA that is larger by a factor of 2.3 times than that of CuO prepared by CHM. Although the HP-CuO has a porous structure, HP-CuO powder seems to be characterized by a low BET-SSA value, which could be due to promoted stacking that is related to post-synthesis processing parameters such as drying and calcination temperature and time.[39] For example, when the hydrated oxide is dried at 80 °C for 12 h and then calcined at a higher temperature of 400 °C for 2 h, this might have promoted the irregular stacking of HP-CuO, as can be seen in SEM images in Figure 1. The irregular stacking of porous structures could lead to the formation of a more stacked and less porous sponge which can cause surface area losses.[40] The stacking might also cause blocking of the pores present in HP-CuO and decrease interlayer spacing which may reduce the uptake of N_2-gas molecules and lower the SSA.[39,41] Nevertheless, the SSA sacrifice apparently due to promoted stacking can be justified by the increase of chemical and thermal stability of the final HP-CuO powder catalyst, as indicated by the TGA measurements shown below. Noteworthy, the low BET-SSA value of HP-CuO is consistent with one study on porous CuO micro-balls,[14] with a reported BET-SSA value of 4.8 m^2/g, which is even >50% less than that of our HP-CuO (10.4 m^2/g).

Figure 4b compares the TGA plots of both MW-synthesized HP-CuO and CuO prepared by CHM. The TGA plots indicate that CuO prepared by the CHM possesses ∼1.4% weight loss after heating to 700 °C, compared to a weight loss of only ∼0.8% in the case of MW-synthesized HP-CuO. The slight weight loss in both cases could arise from the removal of water and hydroxyl groups adsorbed on the surface.[42] Despite the higher porosity of the MW-synthesized HP-CuO compared to the CHM-synthesized CuO as indicated by the SEM and BET results, the HP-CuO also exhibited relatively higher thermal stability, which suggests its tolerance to extreme heat up to 700 °C.

https://doi.org/10.1021/acsomega.2c05399
ACS Omega 2022, 7, 44021−44032

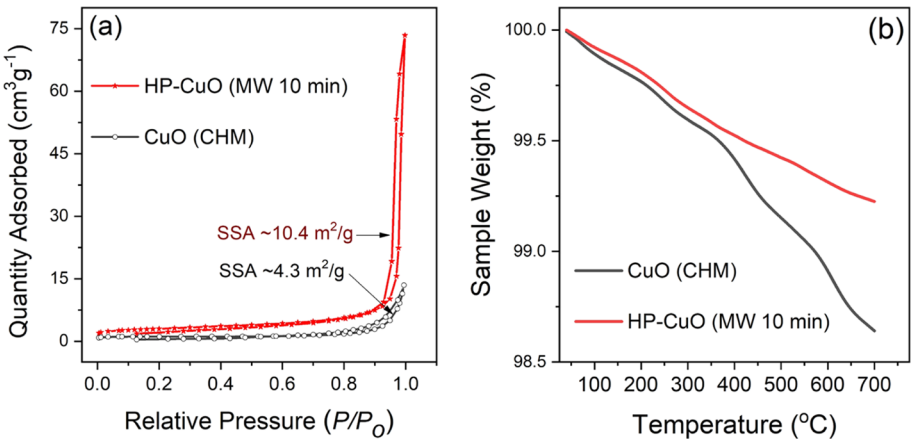

Figure 4. (a) Nitrogen adsorption−desorption isothermal plots and (b) TGA plots of HP-CuO prepared by MWS under MWI for 10 min and the CuO prepared by CHM.

The catalytic activity of heterogeneous catalysts is known to depend on their reducibility properties.[43] Thus, we studied the reducibility of HP-CuO prepared by MWS and CuO prepared by CHM by measuring their TPR profiles in hydrogen (H_2) and carbon monoxide (CO) atmospheres under the same conditions. The H_2-TPR profiles of the MW-synthesized HP-CuO and CHM-synthesized CuO in the temperature range of 100−400 °C are shown in Figure 5a. For the MW-synthesized

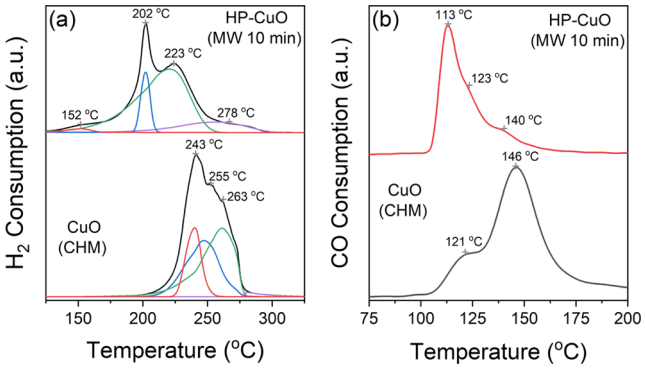

Figure 5. (a) H_2-TPR and (b) CO-TPR profiles of the HP-CuO prepared by MWS under MWI for 10 min and the CuO prepared by CHM.

HP-CuO, four H_2-reduction peaks are observed at reduction temperatures of 155, 202, 223, and 278 °C. The two main H_2-reduction peaks at 202 and 223 °C can be attributed to the reduction of lattice copper species of HP-CuO as Cu(II) → Cu(I) and Cu(I) → Cu.[44] The small H_2-reduction peak at 152 °C could be related to the reduction of exposed fine Cu species on the surface, whereas the one at the highest reduction temperature of 278 °C could be related to unexposed larger Cu entities within the cavities.[45] The CuO prepared by CHM possessed the main H_2-reduction peak at 243 °C along with two higher-temperature reduction peaks at 255 and 263 °C. The lower reduction temperature of the main H_2-reduction peak of HP-CuO (202 °C) compared to CuO (243 °C) indicates the enhanced reducibility of the MW-synthesized HP-CuO and speculates higher catalytic activity in oxidation reactions. Furthermore, the H_2-TPR profiles of CuO and HP-CuO were fitted to calculate the hydrogen consumption for the different H2-TPR peaks of each sample. Figure S4 displays the fitted curves of the H_2-TPR profiles for both CuO and HP-CuO, which reveal 4 fitted peaks in both cases, denoted as α, β, γ, and δ. The data obtained from the fitted curves including temperatures at maxima, H_2 quantities consumed, and % H_2 consumption for CuO and HP-CuO are summarized in Table S1. The calculated % H_2 consumption for the fitted α, β, γ, and δ peaks of CuO was 3.92, 12.32, 68.14, and 15.62%, respectively. For HP-CuO, the % H_2 consumption corresponding to α, β, γ, and δ peaks was 19.22, 34.54, 42.82, and 3.42%, respectively. It can be seen that the largest H_2 consumption represented by peak γ in both HP-CuO (68.14%) and CuO (42.82%) was observed at a lower temperature of 220 °C for HP-CuO compared to 261 °C for CuO. The fitted data indicate that not only the temperature of the main H_2-TPR feature was reduced by a factor of 18% in the case of HP-CuO but also the density of the readily-reducible species was increased by a factor of ∼1.6 compared to that of CuO.

Figure 5b compares the CO-TPR profiles of CuO and HP-CuO samples in the temperature range of 75−200 °C. Comparing the reducibility of the CuO and HP-CuO catalysts in the CO atmosphere indicates that the CO-reduction temperatures of both catalysts follow the order CuO > HP-CuO similar to the order of the H_2-reduction temperatures. The CuO prepared by the CHM showed the main CO-TPR peak at 146 °C besides a small CO-TPR peak at 121 °C. The MW-synthesized HP-CuO by MWI for 10 min possessed the main CO-reduction peak at a much lower temperature of 113 °C and two shoulder CO-reduction peaks at 123 and 140 °C. The general lower reduction temperatures of the MW-synthesized HP-CuO in CO and H_2 atmospheres indicate its higher surface reactivity compared to CuO, which apparently could stem from the enhanced porosity. The TPR findings further support the significance of MW-driven heating in the formation of a hierarchical porous structure with improved physiochemical properties. Thus, the SEM, XRD, BET, TGA, and TPR results confirm that the rational control of morphology and structure of HP-CuO by MWS could modulate the catalyst's reducibility and catalytic performance.[4,8]

The activity of the prepared catalysts for catalytic CO oxidation was studied using a fixed-bed continuous-flow catalytic setup. Figure 6 presents the light-off curves of CO oxidation over the CuO catalyst prepared by CHM and the different MW-synthesized HP-CuO catalysts prepared in

https://doi.org/10.1021/acsomega.2c05399
ACS Omega 2022, 7, 44021−44032

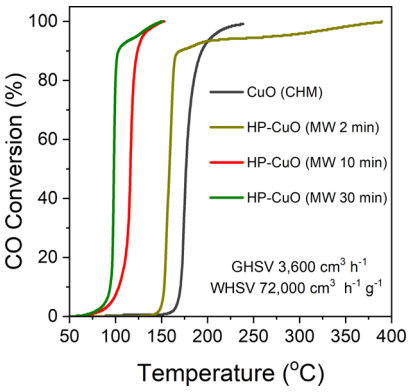

Figure 6. Light-off curves of CO oxidation over the CuO catalyst prepared by the CHM and the different HP-CuO catalysts prepared using MWS reactor under MWI for 2, 10, and 30 min.

closed vials at 130 °C under MWI for 2, 10, and 30 min. Overall, the microwave-synthesized HP-CuO catalysts prepared by MWI for 2, 10, and 30 min outperformed the CuO catalyst prepared by the CHM as determined by the T_{50} and T_{80} of the different catalysts listed in Table S2. The T_{50} and T_{80} denote the catalyst temperature corresponding to CO conversion of 50 and 80%, respectively. The CuO catalyst prepared by CHM possessed T_{50} and T_{80} of 175 and 185 °C, respectively. The CuO catalyst prepared by MWI for 2 min possessed comparatively lowered T_{50} and T_{80} at 157 and 163 °C, respectively. For HP-CuO catalysts where the MWI time was increased to 10 and 30 min, the CO conversion rates were greatly improved. The HP-CuO prepared by MWI for 10 min possessed T_{50} and T_{80} of 115 and 119 °C, respectively, compared to 98 and 100 °C in the case of that prepared by MWI for 30 min. When comparing the temperatures corresponding to 100% CO conversion (T_{100}), it can be stated that the HP-CuO catalysts prepared by MWI for 10 and 30 min exhibited comparable T_{100} of 150 °C, which is relatively much lower than that observed for CuO prepared by the CHM (T_{100} of 240 °C). The CO oxidation results (Figure 6 and Table S2) confirm the higher catalytic activity of the MW-synthesized HP-CuO catalysts in agreement with the enhanced porosity and reducibility properties evident by the BET-SSA (Figure 4a) and TPR measurements (Figure 5). The facile MW-driven synthesis yielded HP-CuO catalysts with an extended hierarchical porosity and 3D sponge-like morphology that promoted the CO oxidation rates under continuous flow. As listed in Table S2, the MW-synthesized HP-CuO catalysts prepared by MWI for 10 and 30 min expressed comparable CO oxidation rates of 35.6 μmol s^{-1} g^{-1} at 150 °C compared to only 0.35 μmol s^{-1} g^{-1} in the case of CuO prepared by CHM at the same temperature. The CO oxidation experiments were carried out under a WHSV of 72,000 cm^3 g^{-1} h^{-1} (Figure 6). The large values of the WHSV and CO oxidation rates of HP-CuO indicate that large CO volumes can be converted per

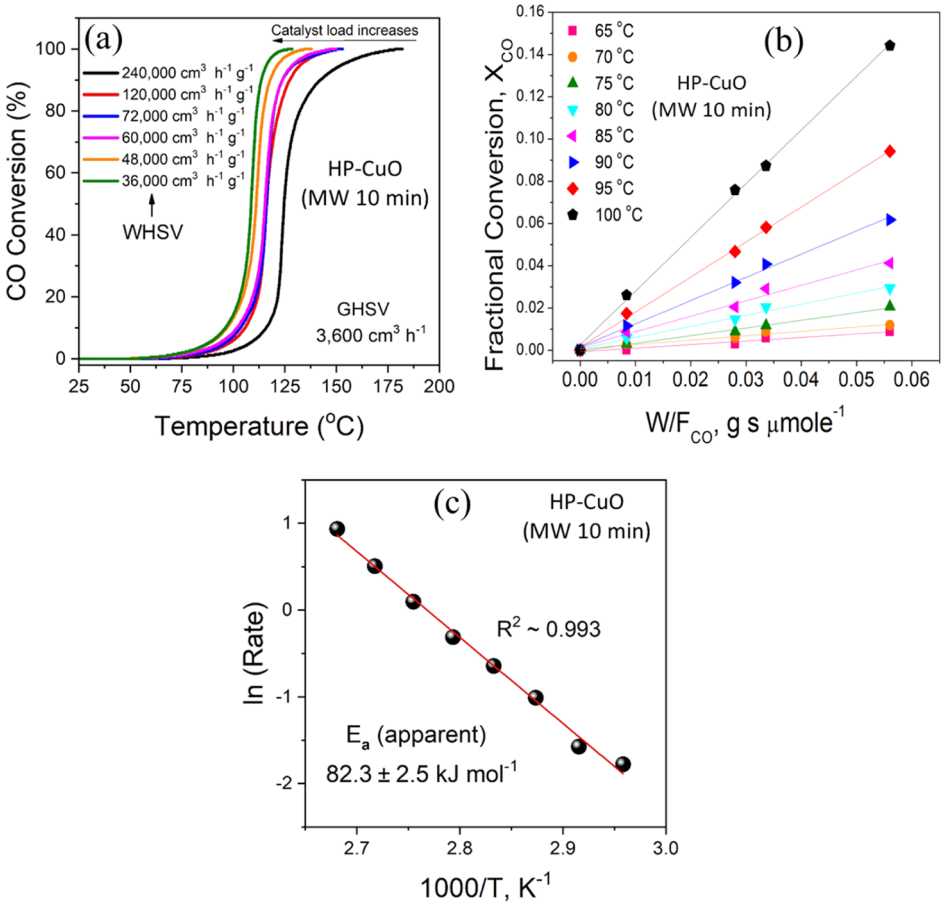

Figure 7. (a) Light-off curves of CO conversion showing the effect of varying the residing time on CO oxidation rates, (b) plots showing the variation in the fractional CO conversion (X_{CO}) with W/F_{CO} ratio, and (c) Arrhenius plot for the HP-CuO catalyst prepared by MWI for 10 min using an MWS reactor.

https://doi.org/10.1021/acsomega.2c05399
ACS Omega 2022, 7, 44021−44032

unit weight of the catalyst at a small residing time. The enhanced CO conversion rates at relatively lower conversion temperatures and smaller residing time can be attributed to the facilitated gas diffusion and the readily reducible surface entities of HP-CuO, as revealed from the TPR results.[46]

We note that the catalytic activity of the HP-CuO reported in this work is indeed comparable to that of some precious metal-based catalysts reported in the literature for CO oxidation. For example, the CuO catalyst reported by Carabineiro et al. expressed full CO conversion at 150 °C only after loading with a gold (Au) co-catalyst.[47] The catalytic activity of the non-precious HP-CuO (T_{100} = 150 °C) is indeed in the same order as that of the precious catalyst Au/CuO. The catalytic behavior of our HP-CuO for CO oxidation is quite similar to that of some precious palladium (Pd) catalysts on ZrO_2[48] and CeO_2-TiO_2[49] supports. Noteworthy, the activity of our HP-CuO (T_{100} = 150 °C) is higher than that reported in a recent study on CuO showing 100% CO conversion at a quite higher temperature of 214 °C employing the same catalyst loading and feed gas ratio.[21] Provided the comparatively lower cost of Cu, this shows the potential of the rational and surfactant-free MWS of HP-CuO at lower cost and processing times as active and inexpensive catalysts for CO oxidation.

To gain some kinetic insights into the CO oxidation reaction over the MW-synthesized HP-CuO catalysts, we studied the influence of the residing time on the catalytic activity of a selected HP-CuO catalyst for CO oxidation reaction. Figure 7a−c displays the light-off curves of CO oxidation under different residing times (Figure 7a), the plots of the CO fractional conversion (X_{CO}) under different W/F_{CO} ratios (Figure 7b), and the Arrhenius plot (Figure 7c) for the HP-CuO catalyst prepared by MWS under MWI for 10 min. The light-off curves of CO oxidation shown in Figure 7a compare the catalytic activity toward CO oxidation under six different WHSV values of 36,000, 48,000, 60,000, 72,000, 120,000, and 240,000 $cm^3\ h^{-1}\ g^{-1}$. Considering the WHSV of 72,000 $cm^3\ h^{-1}\ g^{-1}$ as a middle reference WHSV point, it can be seen that the light-off curves for CO oxidation shift to lower conversion temperatures when decreasing WHSV to 60,000 $cm^3\ h^{-1}\ g^{-1}$ through 48,000 and finally to 36,000 $cm^3\ h^{-1}\ g^{-1}$. The lowered CO conversion temperatures and the subsequent enhanced CO oxidation when decreasing the WHSV can be ascribed to the higher volume density of the active sites on the catalyst surface as the catalyst loading increases. When the WHSV was increased to 120,000 $cm^3\ h^{-1}\ g^{-1}$ and finally up to 240,000 $cm^3\ h^{-1}\ g^{-1}$, the conversion temperatures were also increased due to the higher molar flow of the CO in the feed. The overall trend of the CO oxidation behavior under different WHSV values suggests a good tolerance of the HP-CuO catalyst variation of CO in the feed gas.

We extended the kinetics measurements to the determination of the activation energy of CO oxidation over HP-CuO (MW 10 min) as described in the literature.[17,50] The different kinetic experiments of catalytic CO oxidation were performed by changing the catalyst temperature and loading while maintaining the same molar flow and a fixed GHSV of 3600 $cm^3\ h^{-1}$. The fractional CO conversion (X_{CO}) was determined from the inlet $[F_{CO}]_{in}$ and outlet $[F_{CO}]_{out}$ CO molar flow by using the physical formula of Eq 1

$$X_{CO} = \frac{[F_{CO}]_{in} - [F_{CO}]_{out}}{([F_{CO}]_{in})} \quad (1)$$

The kinetic experiments were conducted in O_2-rich conditions under atmospheric pressure, and data were recorded at a steady state within a differential regime of CO conversion (X_{CO}< 0.2). The reaction rates of CO oxidation (r_{CO}) expressed in the unit of mol $g^{-1}\ s^{-1}$ were determined by using the formula of Eq 2

$$r_{CO}\left(\frac{mol_{CO}}{g_{cat}\ s}\right) = \frac{X_{CO}}{\left(\frac{w}{F_{CO}}\right)} \quad (2)$$

where w is the weight of the catalyst expressed in grams. The determination of the apparent activation energy (E_a) was performed using the Arrhenius plot of ln (r_{CO}) versus $1/T$ based on the reaction rates data collected in the linear range of CO conversion less than 0.2.

Figure 7b,c presents the plots of the change of the fractional CO conversion (X_{CO}) with the W/F_{CO} ratio and the Arrhenius plot (Figure 7c) of the HP-CuO (MW 10 min) catalyst. The (X_{CO}) versus W/F_{CO} plots (Figure 7b) reveal a linear increase of fractional CO conversion with the temperature at a specific fixed W/F_{CO} ratio, where CO oxidation is facilitated at elevated temperatures. The higher CO oxidation activity could arise from the oxygen activation and diffusion on the HP-CuO surface as shown above by the CO-TPR measurements (Figure 5a). This was further supported by XPS measurements that were used to characterize the surface properties of the HP-CuO catalyst and determine the oxidation state of copper in fresh and used samples. Figure S5 displays the XPS high-resolution scan spectra of the Cu 2p and O 1s of the MW-synthesized HP-CuO before (fresh catalyst) and after the CO oxidation reaction (used catalyst). The XPS spectra of the Cu 2p of the fresh and used HP-CuO catalyst (Figure S5a) show the core-level peaks of Cu $2p_{3/2}$ and Cu $2p_{1/2}$ lying in the typical binding energy (BE) ranges of 930−945 and 950−965.0 eV, respectively.[11,51] The main peaks located at 933.2 and 953.2 eV convey the Cu $2p_{3/2}$ and Cu $2p_{1/2}$ core transitions of CuO, respectively. In addition, the shake-up satellite peaks in the range of 938−945 eV (Cu $2p_{3/2}$) and at 961.8 eV (Cu $2p_{1/2}$) further support the prominent presence of the bivalent copper [Cu(II)] species.[22,51] In the case of both fresh and used catalysts, the difference between the Cu $2p_{3/2}$ and the Cu $2p_{3/2}$ peaks is 20.0 eV, which further confirms the existence of the pure CuO phase as reported in the literature.[22] This also indicates that no deteriorations in surface properties or phase are observed upon the CO oxidation reaction, which confirms the structural stability of the HP-CuO catalyst. The core-level XPS scan spectra of O 1s for both fresh and used HP-CuO catalysts are compared in Figure S5b. The pronounced peaks located at 529.6 and 529.5 eV for fresh and used catalysts, respectively, correspond to the oxygen ions involved in the lattice metal−oxygen bond of CuO.[4,14] The shoulder peak observed at around 528.3 eV in the case of the fresh calcined HP-CuO can be assigned to the O^{2-} ions, as indicated earlier by Wu et al.[52] For the used HP-CuO catalyst, a broad XPS peak could be observed at about 531.5 eV, which can be ascribed to adsorbed oxygen species of hydroxyl anions present on the surface.[14] Furthermore, the core-level transitions of the O 1s of chemically adsorbed hydroxide and carbonate species typically appear in the range of 531−532 eV.[17] Accordingly, the peak at 531.5 eV could also be related to the carbonate or polarized oxygen ions adjacent to oxygen (O) vacant sites or bonded oxygen in the used HP-CuO

https://doi.org/10.1021/acsomega.2c05399
ACS Omega 2022, 7, 44021−44032

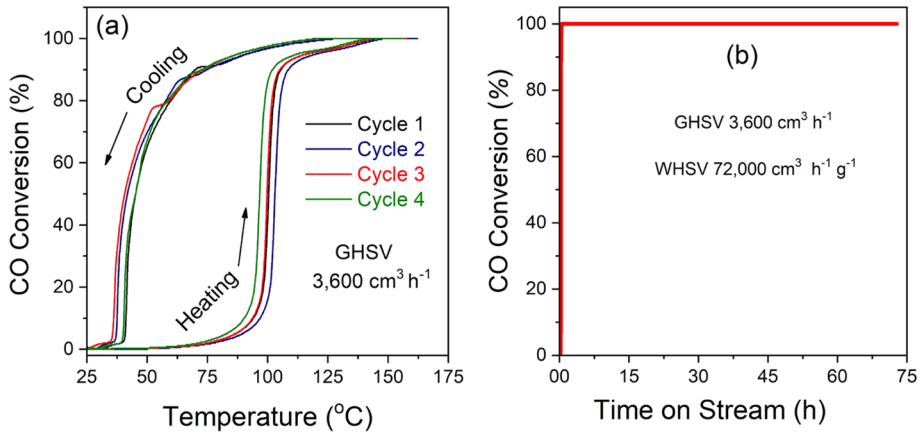

Figure 8. (a) Plots of CO conversion vs temperature showing cycling stability and (b) plot of CO conversion vs time showing long-term stability of CO oxidation for 72 h on the stream over the HP-CuO (MW 10 min) catalyst prepared by MWS.

catalyst.[4,9] The high BE peak at 531.5 was only observed in the case of the used HP-CuO catalyst, which infers the presence of oxygen vacant sites and indicates their role in the enhanced CO oxidation.

The TPR, XPS, and catalysis results support the presence of readily available active surface oxygen species on HP-CuO at low temperatures. It is also evident that the catalytic CO oxidation depends on the catalysis residing time expressed in terms of W/F_{CO} (W = weight of the catalyst in grams and F_{CO} = molar flow rate in μmol s^{-1}), as can be seen in Figure 7b. At a given catalyst temperature and under a fixed GHSV of 3600 h^{-1}, the fractional CO conversion increases as the residing time increases, since more active sites are readily available.[53] The CO oxidation reaction can follow various kinetics and reaction rates of positive or negative order, and thus, a broad range of apparent activation energies (E_a) is known in the literature.[53,54] Figure 7c shows the Arrhenius plot corresponding to the HP-CuO catalyst prepared by MWI for 10 min. The experimental value of the apparent activation energy (E_a) determined by using the Arrhenius plot was found to be ~82 kJ $mol,^{-1}$ which speculates a strong adsorption and bond energy of CO to the HP-CuO surface.[54] It can be stated that the CO oxidation reaction over the HP-CuO catalysts follows the Langmuir–Hinshelwood (L–H) reaction mechanism in which the reaction between the adsorbed CO molecules and co-adsorbed O atoms takes place on the CuO surface as outlined in Eqs 3–5.[51,55]

$$CO_{(gaseous)} + Cu_{(surface)} \rightarrow CO - Cu_{(surface)} \quad (3)$$

$$O_{2(gaseous)} + Cu_{(surface)} - Cu_{(surface)} \rightarrow 2O - Cu_{(surface)} \quad (4)$$

$$CO - Cu_{(surface)} + O - Cu_{(surface)} \rightarrow CO_{2(gaseous)} + Cu_{(surface)} - Cu_{(surface)} \quad (5)$$

The stability of a heterogeneous catalyst is crucial for the continuous availability of the active sites on its surface, thus attaining a stable catalytic performance for the CO oxidation reaction. As discussed above, the XPS measurements of the Cu 2p and O 1s of HP-CuO before and after CO oxidation (Figure S5) confirmed the structural and chemical stability of the copper and oxygen species in HP-CuO. The phase stability of the HP-CuO catalyst was investigated by the measurement of the XRD patterns of HP-CuO before and after the catalytic reaction. Figure S6 presents the XRD patterns of fresh (calcined) and used (as is after CO oxidation reaction) HP-CuO catalyst. The patterns confirm the pure crystallinity and stability of the monoclinic phase HP-CuO upon CO oxidation reaction. Furthermore, the cycling- and long-term stabilities of the CO oxidation over the HP-CuO (MW 10 min) catalyst were also investigated. Figure 8a shows overlaid plots of CO conversion versus temperature for 4 consecutive CO oxidation cycles over HP-CuO (MW 10 min) with programmed heating and natural cooling of the catalyst bed. The steady temperature corresponding to 100% CO conversion and the close matching of the 4 catalytic CO oxidation cycles indicate the good cycling stability of HP-CuO. Figure 8b shows the long-term stability plot of CO oxidation over HP-CuO (MW 10 min) for 72 h on the stream. The CO feed was passed over the catalyst at a flow rate of 60 cm^3 min^{-1}, which corresponds to a WHSV of 72,000 cm^3 h^{-1} g^{-1}. Then, the catalyst temperature was ramped until a 100% CO conversion was achieved (150 °C). Finally, the catalyst was maintained at this temperature for 72 h under constant flow with continuous monitoring of the CO conversion. The HP-CuO catalyst possessed a stable catalytic performance with a steady 100% CO conversion for 3 days without deactivation or stability compromise. The cycling- and long-term stability measurements confirm the good resistance of the HP-CuO catalyst to poisoning or deactivation. The above analysis, catalysis, kinetic, and stability results indicate that HP-CuO catalysts prepared by MWS could serve as inexpensive, durable, highly stable, and efficient catalysts for CO oxidation reactions at low temperatures.

4. CONCLUSIONS

In conclusion, a rapid and facile microwave-driven method for the rational synthesis of hierarchical porous copper oxide (HP-CuO) with a sponge-like morphology is described. The microwave-synthesized HP-CuO featured interesting physical and chemical properties including larger porosity and specific surface, higher thermal stability, and improved reducibility compared to CuO prepared by the CHM. The structure–property relationships and their impact on catalytic activity were emphasized by CO oxidation measurements over HP-CuO. The HP-CuO catalysts expressed enhanced CO conversion rates with a 100% CO conversion at 150 °C. The HP-CuO catalyst prepared by MWS for 10 min exhibited a CO oxidation reaction rate of 35.6 μmol s^{-1} g^{-1} at 150 °C and

https://doi.org/10.1021/acsomega.2c05399
ACS Omega 2022, 7, 44021–44032

apparent activation energy of 82 kJ mol^{-1}. Moreover, the HP-CuO catalyst expressed high long-term stability for multiple cycles. The microwave-assisted synthetic approach reported herein introduces a unique and simple method for the controlled preparation of porous, active, and stable copper-based catalysts for low-temperature CO oxidation.

■ ASSOCIATED CONTENT

Supporting Information

The Supporting Information is available free of charge at https://pubs.acs.org/doi/10.1021/acsomega.2c05399.

FE-SEM micrograph images of CuO prepared by CHM using an aqueous mixture of copper nitrate and carbamide of 1:8 molar ratio similar to the MWS; XRD patterns of CuO prepared by CHM and HP-CuO prepared using MWS reactor under MWI for 10 min; Raman spectrum of HP-CuO; experimental and fitted curves of the H_2-TPR profiles of HP-CuO and CuO; summary of the fitted H_2-TPR peaks showing corresponding temperatures at maxima and % H_2 consumption for CuO and HP-CuO; summary of the catalysts temperatures corresponding to 50, 80, and 100% CO conversion and values of the CO oxidation reaction rates of the different catalysts; XPS scan spectra of Cu 2p and O 1s of HP-CuO (MW 10 min) before and after the CO oxidation reaction; and XRD spectra of the HP-CuO catalyst prepared using the MWS reactor under MWI for 10 min showing patterns of the fresh and used catalysts (PDF)

■ AUTHOR INFORMATION

Corresponding Authors

Abdallah F. Zedan − *National Institute of Laser Enhanced Sciences, Cairo University, Giza 12613, Egypt; Department of Chemistry, Virginia Commonwealth University, Richmond, Virginia 23284, United States;* orcid.org/0000-0002-5241-9917; Email: zedanabdallah@cu.edu.eg

M. Samy El-Shall − *Department of Chemistry, Virginia Commonwealth University, Richmond, Virginia 23284, United States;* orcid.org/0000-0002-1013-4948; Email: mselshal@vcu.edu

Author

Amina S. AlJaber − *Department of Chemistry and Earth Sciences, Qatar University, Doha 2713, Qatar*

Complete contact information is available at: https://pubs.acs.org/10.1021/acsomega.2c05399

Notes

The authors declare no competing financial interest.

■ ACKNOWLEDGMENTS

This work was supported by grant no. NPRP 8-1912-1-354 from the QNRF (a member of the Qatar Foundation). We also thank the support from the National Science Foundation (CHE-1900094), Mary Eugenia Kapp's Chair Endowment, and NILES.

■ REFERENCES

(1) (a) Polychronopoulou, K.; AlKhoori, A. A.; Efstathiou, A. M.; Jaoude, M. A.; Damaskinos, C. M.; Baker, M. A.; Almutawa, A.; Anjum, D. H.; Vasiliades, M. A.; Belabbes, A.; et al. Design Aspects of Doped CeO2 for Low-Temperature Catalytic CO Oxidation: Transient Kinetics and DFT Approach. *ACS Appl. Mater. Interfaces* **2021**, *13*, 22391−22415. (b) Basina, G.; Polychronopoulou, K.; Zedan, A. F.; Dimos, K.; Katsiotis, M. S.; Fotopoulos, A. P.; Ismail, I.; Tzitzios, V. Ultrasmall Metal-Doped CeO2 Nanoparticles for Low-Temperature CO Oxidation. *ACS Appl. Nano Mater.* **2020**, *3*, 10805−10813.

(2) (a) Du, C.; Lu, G.; Guo, Y.; Guo, Y.; Gong, X.-q. Surfactant-Mediated One-Pot Method To Prepare Pd−CeO2 Colloidal Assembled Spheres and Their Enhanced Catalytic Performance for CO Oxidation. *ACS Omega* **2016**, *1*, 118−126. (b) Brindle, J.; Nigra, M. M. Compensation Effect Exhibited by Gold Bimetallic Nanoparticles during CO Oxidation. *ACS Omega* **2021**, *6*, 24269−24279.

(3) Zedan, A. F.; Allam, N. K.; AlQaradawi, S. Y. A Study of Low-Temperature CO Oxidation over Mesoporous CuO-TiO2 Nanotube Catalysts. *Catalysts* **2017**, *7*, 129.

(4) Zedan, A. F.; Gaber, S.; AlJaber, A. S.; Polychronopoulou, K. CO Oxidation at Near-Ambient Temperatures over TiO2-Supported Pd-Cu Catalysts: Promoting Effect of Pd-Cu Nanointerface and TiO2 Morphology. *Nanomaterials* **2021**, *11*, 1675.

(5) (a) Gawande, M. B.; Goswami, A.; Felpin, F.-X.; Asefa, T.; Huang, X.; Silva, R.; Zou, X.; Zboril, R.; Varma, R. S. Cu and Cu-Based Nanoparticles: Synthesis and Applications in Catalysis. *Chem. Rev.* **2016**, *116*, 3722−3811. (b) Wang, Y.; Wen, Z. H.; Zhang, H. L.; Cao, G. H.; Sun, Q.; Cao, J. L. CuO Nanorods-Decorated Reduced Graphene Oxide Nanocatalysts for Catalytic Oxidation of CO. *Catalysts* **2016**, *6*, 214.

(6) (a) AlKhoori, A. A.; Polychronopoulou, K.; Belabbes, A.; Jaoude, M.; Vega, L. F.; Sebastian, V.; Hinder, S. S.; Baker, M. A.; Zedan, A. F. Cu, Sm Co-Doping effect on the CO oxidation activity of CeO2. A combined experimental and density functional study. *Appl. Surf. Sci.* **2020**, *521*, 146305. (b) AlKetbi, M.; Polychronopoulou, K.; Abi Jaoude, M.; Vasiliades, M. A.; Sebastian, V.; Hinder, S. J.; Baker, M. A.; Zedan, A. F.; Efstathiou, A. M. Cu-Ce-La-Ox as efficient CO oxidation catalysts: Effect of Cu content. *Appl. Surf. Sci.* **2020**, *505*, 144474.

(7) Zedan, A. F.; AlJaber, A. S. Combustion Synthesis of Non-Precious CuO-CeO2 Nanocrystalline Catalysts with Enhanced Catalytic Activity for Methane Oxidation. *Materials* **2019**, *12*, 878.

(8) Zedan, A. F.; Polychronopoulou, K.; Asif, A.; AlQaradawi, S. Y.; AlJaber, A. S. Cu-Ce-O catalyst revisited for exceptional activity at low temperature CO oxidation reaction. *Surf. Coat. Technol.* **2018**, *354*, 313−323.

(9) AlKetbi, M.; Polychronopoulou, K.; Zedan, A. F.; Sebastián, V.; Baker, M. A.; AlKhoori, A.; Jaoude, M.; Alnuaimi, O.; Hinder, S. S.; Tharalekshmy, A.; AlJaber, A. S. Tuning the activity of Cu-containing rare earth oxide catalysts for CO oxidation reaction: Cooling while heating paradigm in microwave-assisted synthesis. *Mater. Res. Bull.* **2018**, *108*, 142−150.

(10) (a) Sonobe, K.; Tanabe, M.; Yamamoto, K. Enhanced Catalytic Performance of Subnano Copper Oxide Particles. *ACS Nano* **2020**, *14*, 1804−1810. (b) Hong, K.; Suh, J. M.; Lee, T. H.; Cho, S. H.; Ramakrishna, S.; Varma, R. S.; Jang, H. W.; Shokouhimehr, M. Architecture engineering of nanostructured catalyst via layer-by-layer adornment of multiple nanocatalysts on silica nanorod arrays for hydrogenation of nitroarenes. *Sci. Rep.* **2022**, *12*, 2. (c) Mao, J.; Qin, L.; Tian, L.; He, L.; Zhu, Y.; Meng, Q.; Zhang, G. Hierarchical N-Doped CuO/Cu Composites Derived from Dual-Ligand Metal−Organic Frameworks as Cost-Effective Catalysts for Low-Temperature CO Oxidation. *ACS Omega* **2021**, *6*, 29596−29608.

(11) Zhang, X.; Li, G.; Yang, S.; Song, X.; Sun, Z. Nanoporous CuO ribbons modified by Au nanoparticles through chemical dealloying and calcination for CO oxidation. *Microporous Mesoporous Mater.* **2016**, *226*, 61−70.

(12) (a) Deka, P.; Deka, R. C.; Bharali, P. Porous CuO nanostructure as a reusable catalyst for oxidative degradation of organic water pollutants. *New J. Chem.* **2016**, *40*, 348−357. (b) Shi, L.; Yang, C.; Su, X.; Wang, J.; Xiao, F.; Fan, J.; Feng, C.; Sun, H. Microwave-hydrothermal synthesis of CuO nanorods and their

catalytic applications in sodium humate synthesis and RhB degradation. *Ceram. Int.* **2014**, *40*, 5103−5106. (c) Sun, S.; Zhang, X.; Yang, Q.; Liang, S.; Zhang, X.; Yang, Z. Cuprous oxide (Cu2O) crystals with tailored architectures: A comprehensive review on synthesis, fundamental properties, functional modifications and applications. *Prog. Mater. Sci.* **2018**, *96*, 111−173. (d) Yang, Z.; Zhang, L.; Zhang, Y.; Zhao, Y.; Jing, L.; Yan, Y.; Sun, K. Rational design of CuO@Cu nanostructure with tuneable morphology and electrochemical properties. *RSC Adv.* **2014**, *4*, 8121−8124.

(13) Sang, X.; Zhang, J.; Wu, T.; Zhang, B.; Ma, X.; Peng, L.; Han, B.; Kang, X.; Liu, C.; Yang, G. Room-temperature synthesis of mesoporous CuO and its catalytic activity for cyclohexene oxidation. *RSC Adv.* **2015**, *5*, 67168−67174.

(14) Subalakshmi, P.; Ganesan, M.; Sivashanmugam, A. Synthesis of 3D architecture CuO micro balls and nano hexagons and its electrochemical capacitive behavior. *Mater. Des.* **2017**, *119*, 104−112.

(15) (a) Bhagat, M.; Anand, R.; Sharma, P.; Rajput, P.; Sharma, N.; Singh, K. Review—Multifunctional Copper Nanoparticles: Synthesis and Applications. *ECS J. Solid State Sci. Technol.* **2021**, *10*, 063011. (b) Yang, C.; Su, X. T.; Wang, J. D.; Cao, X. D.; Wang, S. J.; Zhang, L. Facile microwave-assisted hydrothermal synthesis of varied-shaped CuO nanoparticles and their gas sensing properties. *Sens. Actuators, B* **2013**, *185*, 159−165. (c) Ye, J.; Li, Z.; Dai, Z.; Zhang, Z.; Guo, M.; Wang, X. Facile Synthesis of Hierarchical CuO Nanoflower for Supercapacitor Electrodes. *J. Electron. Mater.* **2016**, *45*, 4237−4245.

(16) (a) Awad, F. S.; Kiriarachchi, H. D.; AbouZeid, K. M.; Özgür, Ü.; El-Shall, M. S. Plasmonic Graphene Polyurethane Nanocomposites for Efficient Solar Water Desalination. *ACS Appl. Energy Mater.* **2018**, *1*, 976−985. (b) Elazab, H. A.; Moussa, S.; Siamaki, A. R.; Gupton, B. F.; El-Shall, M. S. The Effect of Graphene on Catalytic Performance of Palladium Nanoparticles Decorated with Fe3O4, Co3O4, and Ni (OH)2: Potential Efficient Catalysts Used for Suzuki Cross—Coupling. *Catal. Lett.* **2017**, *147*, 1510−1522. (c) Zedan, A. F.; Abdelsayed, V.; Mohamed, M. B.; El-Shall, M. S. Rapid synthesis of magnetic/luminescent (Fe 3 O 4/CdSe) nanocomposites by microwave irradiation. *J. Nanopart. Res.* **2013**, *15*, 1312.

(17) Polychronopoulou, K.; Zedan, A. F.; Katsiotis, M. S.; Baker, M. A.; AlKhoori, A. A.; AlQaradawi, S. Y.; Hinder, S. J.; AlHassan, S. Rapid microwave assisted sol-gel synthesis of CeO 2 and Ce x Sm 1-x O 2 nanoparticle catalysts for CO oxidation. *Mol. Catal.* **2017**, *428*, 41−55.

(18) Goel, S.; Tomar, A. K.; Sharma, R. K.; Singh, G. Highly Pseudocapacitive NiO Nanoflakes through Surfactant-Free Facile Microwave-Assisted Route. *ACS Appl. Energy Mater.* **2018**, *1*, 1540−1548.

(19) Herring, N. P.; Panchakarla, L. S.; El-Shall, M. S. P-Type Nitrogen-Doped ZnO Nanostructures with Controlled Shape and Doping Level by Facile Microwave Synthesis. *Langmuir* **2014**, *30*, 2230−2240.

(20) (a) Davó-Quiñonero, A.; Bailón-García, E.; López-Rodríguez, S.; Juan-Juan, J.; Lozano-Castelló, D.; García-Melchor, M.; Herrera, F. C.; Pellegrin, E.; Escudero, C.; Bueno-López, A. Insights into the Oxygen Vacancy Filling Mechanism in CuO/CeO2 Catalysts: A Key Step Toward High Selectivity in Preferential CO Oxidation. *ACS Catal.* **2020**, *10*, 6532−6545. (b) Lin, L.; Shi, P.; Yao, L.; Xie, K.; Tao, H.; Zhang, Z.; Wang, Y. First-principles study on CO oxidation on CuO(111) surface prefers the Eley−Rideal or Langmuir−Hinshelwood pathway. *Nanotechnology* **2022**, *33*, 205504.

(21) Khder, A. S.; Ahmed, S. A.; Altass, H. M.; Morad, M.; Ibrahim, A. A. CO oxidation over nobel metals supported on copper oxide: effect of Cu+/Cu2+ ratio. *J. Mater. Res. Technol.* **2020**, *9*, 14200−14211.

(22) Ghosh, S.; Kundu, S.; Naskar, M. K. Mesoporous CuO nanostructures for low-temperature CO oxidation. *Bull. Mater. Sci.* **2021**, *44*, 189.

(23) Zhu, Y.-J.; Chen, F. Microwave-Assisted Preparation of Inorganic Nanostructures in Liquid Phase. *Chem. Rev.* **2014**, *114*, 6462−6555.

(24) Qiu, G.; Dharmarathna, S.; Zhang, Y.; Opembe, N.; Huang, H.; Suib, S. L. Facile Microwave-Assisted Hydrothermal Synthesis of CuO Nanomaterials and Their Catalytic and Electrochemical Properties. *J. Phys. Chem. C* **2012**, *116*, 468−477.

(25) Zedan, A. F.; Mohamed, A. T.; El-Shall, M. S.; AlQaradawi, S. Y.; AlJaber, A. S. Tailoring the reducibility and catalytic activity of CuO nanoparticles for low temperature CO oxidation. *RSC Adv.* **2018**, *8*, 19499−19511.

(26) Polychronopoulou, K.; Zedan, A. F.; AlKetbi, M.; Stephen, S.; Ather, M.; Katsiotis, M. S.; Arvanitidis, J.; Christofilos, D.; Isakovic, A. F.; AlHassan, S. Tailoring the efficiency of an active catalyst for CO abatement through oxidation reaction: The case study of samarium-doped ceria. *J. Environ. Chem. Eng.* **2018**, *6*, 266−280.

(27) Zedan, A. F.*Graphene-Based Semiconductor and Metallic Nanostructured Materials*; Virginia Commonwealth University: USA, 2013.

(28) (a) Yang, C.; Xiao, F.; Wang, J.; Su, X. 3D flower- and 2D sheet-like CuO nanostructures: Microwave-assisted synthesis and application in gas sensors. *Sens. Actuators, B* **2015**, *207*, 177−185. (b) Zedan, A. F.; Sappal, S.; Moussa, S.; El-Shall, M. S. Ligand-Controlled Microwave Synthesis of Cubic and Hexagonal CdSe Nanocrystals Supported on Graphene. Photoluminescence Quenching by Graphene. *J. Phys. Chem. C* **2010**, *114*, 19920−19927.

(29) Naikoo, G. A.; Dar, R. A.; Khan, F. Hierarchically macro/mesostructured porous copper oxide: facile synthesis, characterization, catalytic performance and electrochemical study of mesoporous copper oxide monoliths. *J. Mater. Chem. A* **2014**, *2*, 11792−11798.

(30) Šubrt, J.; Štengl, V.; Bakardjieva, S.; Szatmary, L. Synthesis of spherical metal oxide particles using homogeneous precipitation of aqueous solutions of metal sulfates with urea. *Powder Technol.* **2006**, *169*, 33−40.

(31) Xue, H.; Zhang, W.; Li, X.; You, X.; Rao, J.; Pan, F. A facile green synthesis of Sm2O3 nanoparticles via microwave-assisted urea precipitation route and their optical properties. *Electron. Mater. Lett.* **2017**, *13*, 255−259.

(32) Seza, A.; Soleimani, F.; Naseri, N.; Soltaninejad, M.; Montazeri, S. M.; Sadrnezhaad, S. K.; Mohammadi, M. R.; Moghadam, H. A.; Forouzandeh, M.; Amin, M. H. Novel microwave-assisted synthesis of porous g-C3N4/SnO2 nanocomposite for solar water-splitting. *Appl. Surf. Sci.* **2018**, *440*, 153−161.

(33) Hosseini H, S. M.; Siavash Moakhar, R.; Soleimani, F.; Sadrnezhaad, S. K.; Masudy-Panah, S.; Katal, R.; Seza, A.; Ghane, N.; Ramakrishna, S. One-pot microwave synthesis of hierarchical C-doped CuO dandelions/g-C3N4 nanocomposite with enhanced photostability for photoelectrochemical water splitting. *Appl. Surf. Sci.* **2020**, *530*, 147271.

(34) Sun, M.-H.; Chen, L.-H.; Su, B.-L.Hierarchically Structured Porous Materials. *The Sol-Gel Handbook*; Wiley, 2015; pp 987−1030.

(35) (a) Laha, S.; Chakraborty, A.; Maji, T. K. Synergistic Role of Microwave and Perturbation toward Synthesis of Hierarchical Porous MOFs with Tunable Porosity. *Inorg. Chem.* **2020**, *59*, 3775−3782. (b) Zhu, Y.; Cao, C.; Tao, S.; Chu, W.; Wu, Z.; Li, Y. Ultrathin Nickel Hydroxide and Oxide Nanosheets: Synthesis, Characterizations and Excellent Supercapacitor Performances. *Sci. Rep.* **2014**, *4*, 5787.

(36) Zedan, M.; Zedan, A. F.; Amin, R. M.; Li, X. Visible-light active metal nanoparticles@carbon nitride for enhanced removal of water organic pollutants. *J. Environ. Chem. Eng.* **2022**, *10*, 107780.

(37) Ethiraj, A. S.; Kang, D. J. Synthesis and characterization of CuO nanowires by a simple wet chemical method. *Nanoscale Res. Lett.* **2012**, *7*, 70.

(38) Huang, H.; Zhang, L.; Wu, K.; Yu, Q.; Chen, R.; Yang, H.; Peng, X.; Ye, Z. Hetero-metal cation control of CuO nanostructures and their high catalytic performance for CO oxidation. *Nanoscale* **2012**, *4*, 7832−7841.

(39) Hoar, E.; Shehee, T. C.; Roy, L. E. Impact of Precipitation Parameters on the Specific Surface Area of PuO2. *ACS Omega* **2022**, *7*, 540−547.

https://doi.org/10.1021/acsomega.2c05399
ACS Omega 2022, 7, 44021−44032

(40) Guo, F.; Creighton, M.; Chen, Y.; Hurt, R.; Külaots, I. Porous structures in stacked, crumpled and pillared graphene-based 3D materials. *Carbon* **2014**, *66*, 476−484.
(41) Walton, K. S.; Snurr, R. Q. Applicability of the BET Method for Determining Surface Areas of Microporous Metal−Organic Frameworks. *J. Am. Chem. Soc.* **2007**, *129*, 8552−8556.
(42) Ganesh, I.; Kumar, P. P.; Annapoorna, I.; Sumliner, J. M.; Ramakrishna, M.; Hebalkar, N. Y.; Padmanabham, G.; Sundararajan, G. Preparation and characterization of Cu-doped TiO2 materials for electrochemical, photoelectrochemical, and photocatalytic applications. *Appl. Surf. Sci.* **2014**, *293*, 229−247.
(43) Jang, M. G.; Yoon, S.; Shin, D.; Kim, H. J.; Huang, R.; Yang, E.; Kim, J.; Lee, K.-S.; An, K.; Han, J. W. Boosting Support Reducibility and Metal Dispersion by Exposed Surface Atom Control for Highly Active Supported Metal Catalysts. *ACS Catal.* **2022**, *12*, 4402−4414.
(44) Sonobe, K.; Tanabe, M.; Imaoka, T.; Chun, W.-J.; Yamamoto, K. Low-Temperature H2 Reduction of Copper Oxide Subnanoparticles. *Chem. Eur. J* **2021**, *27*, 8452−8456.
(45) (a) Hossain, S. T.; Azeeva, E.; Zhang, K.; Zell, E. T.; Bernard, D. T.; Balaz, S.; Wang, R. A comparative study of CO oxidation over Cu-O-Ce solid solutions and CuO/CeO2 nanorods catalysts. *Appl. Surf. Sci.* **2018**, *455*, 132−143. (b) Zeng, S.; Zhang, W.; Śliwa, M.; Su, H. Comparative study of CeO2/CuO and CuO/CeO2 catalysts on catalytic performance for preferential CO oxidation. *Int. J. Hydrogen Energy* **2013**, *38*, 3597−3605.
(46) Carrettin, S.; Hao, Y.; Aguilar-Guerrero, V.; Gates, B. C.; Trasobares, S.; Calvino, J. J.; Corma, A. Increasing the Number of Oxygen Vacancies on TiO2 by Doping with Iron Increases the Activity of Supported Gold for CO Oxidation. *Chem. Eur. J* **2007**, *13*, 7771−7779.
(47) Carabineiro, S. A. C.; Bogdanchikova, N.; Avalos-Borja, M.; Pestryakov, A.; Tavares, P. B.; Figueiredo, J. L. Gold supported on metal oxides for carbon monoxide oxidation. *Nano Res.* **2011**, *4*, 180−193.
(48) Vedyagin, A. A.; Volodin, A. M.; Kenzhin, R. M.; Chesnokov, V. V.; Mishakov, I. V. CO Oxidation over Pd/ZrO(2) Catalysts: Role of Support's Donor Sites. *Molecules* **2016**, *21*, 1289.
(49) Satsuma, A.; Yanagihara, M.; Osaki, K.; Saeki, Y.; Liu, H.; Yamamoto, Y.; Arai, S.; Ohyama, J. Promotion of low-temperature oxidation of CO over Pd supported on titania-coated ceria. *RSC Adv.* **2014**, *4*, 54187−54193.
(50) Ayastuy, J. L.; Gurbani, A.; González-Marcos, M. P.; Gutiérrez-Ortiz, M. A. Kinetics of Carbon Monoxide Oxidation over CuO Supported on Nanosized CeO2. *Ind. Eng. Chem. Res.* **2009**, *48*, 5633−5641.
(51) Bu, Y.; Niemantsverdriet, J. W. H.; Fredriksson, H. O. A. Cu Model Catalyst Dynamics and CO Oxidation Kinetics Studied by Simultaneous in Situ UV−Vis and Mass Spectroscopy. *ACS Catal.* **2016**, *6*, 2867−2876.
(52) Wu, L. Q.; Li, Y. C.; Li, S. Q.; Li, Z. Z.; Tang, G. D.; Qi, W. H.; Xue, L. C.; Ge, X. S.; Ding, L. L. Method for estimating ionicities of oxides using O1s photoelectron spectra. *AIP Adv.* **2015**, *5*, 097210.
(53) Singh, S. A.; Madras, G. Detailed mechanism and kinetic study of CO oxidation on cobalt oxide surfaces. *Appl. Catal., A* **2015**, *504*, 463−475.
(54) Jia, A.-P.; Deng, Y.; Hu, G.-S.; Luo, M.-F.; Lu, J.-Q. Kinetic and activity study of CO oxidation over CuO−MnOx−CeO2 catalysts. *React. Kinet. Mech. Catal.* **2016**, *117*, 503−520.
(55) Royer, S.; Duprez, D. Catalytic Oxidation of Carbon Monoxide over Transition Metal Oxides. *ChemCatChem* **2011**, *3*, 24−65.

https://doi.org/10.1021/acsomega.2c05399
ACS Omega 2022, 7, 44021−44032